International Journal of Thermophysics (2022) 43: 167
https://doi.org/10.1007/s10765-022-03084-z

Effective Thermal Conductivity of Nanofluids Containing Silicon Dioxide or Zirconium Dioxide Nanoparticles Dispersed in a Mixture of Water and Glycerol

Francisco E. Berger Bioucas[1] · Christian Köhn[2] · Annelise Jean-Fulcrand[2] · Georg Garnweitner[2] · Thomas M. Koller[1] · Andreas P. Fröba[1]

Received: 8 August 2022 / Accepted: 12 August 2022 / Published online: 12 September 2022

Abstract

The present study investigates the effective thermal conductivity of nanofluids containing crystalline or amorphous silicon dioxide (SiO_2), or zirconium dioxide (ZrO_2) nanoparticles dispersed in a mixture of water and glycerol with a mass ratio of 60:40. Such fluids are relevant as potential cutting fluids in tribology and feature a broad distribution of irregularly shaped non-spherical particles of dimensions on the order of (100 to 200) nm that were produced by comminution of larger particles or particle aggregates. A new steady-state guarded parallel-plate instrument was applied for the absolute measurement of the effective thermal conductivity of the nanofluids with an expanded uncertainty (coverage factor $k=2$) of 3% for temperatures from (293 to 353) K and particle volume fractions up to 0.1. For a constant volume fraction of 0.03 for the three particle types, the measured thermal-conductivity ratios, i.e. the effective thermal conductivity of the nanofluids relative to the thermal conductivity of the base fluid, are less than 1.05 and not affected by temperature. In the case of the nanofluids with crystalline SiO_2, with increasing particle volume fraction from 0.03 to 0.10 the thermal-conductivity ratios increase up to values of about 1.18 for all temperatures. A comparison of the measurement results with the Hamilton-Crosser model and an analytical resistance model for the effective thermal conductivity of nanofluids shows that the former one allows for better predictions for the present nanofluids with a relatively large viscosity. In this context, it could be shown that detailed knowledge about the sphericity and thermal conductivity of the dispersed nanoparticles is required for the modeling approaches.

Keywords Cutting fluids · Effective thermal conductivity · Metal-oxide nanoparticles · Nanofluids · Parallel-plate method · Prediction

✉ Andreas P. Fröba
andreas.p.froeba@fau.de

Extended author information available on the last page of the article

1 Introduction

According to the original work of Choi and Eastman [1], nanofluids consist of a liquid continuous dispersion medium and a dispersed phase of solid nanoparticles with dimensions in the nanometer range. The application of nanofluids is highly versatile due to their extensive range of properties and tailorability. The classical field of potential application is the use of nanofluids as heat transfer fluids in heat exchangers [2–5]. Since the effective thermal conductivity of nanofluids as one key thermophysical property in heat engineering is typically larger than the thermal conductivity of the particle-free base fluids, the overall heat transfer can be increased [5]. In a recent review [6] on the heat transfer capabilities of nanofluids in a tube-bundle heat exchanger, however, the conclusion was drawn that the benefits in the overall heat transfer are rather modest when replacing a conventional fluid by a nanofluid.

In recent years, the usage of nanofluids as cutting fluids in machining processes became popular [7–10]. Minimum quantity lubrication (MQL) which needs only small amounts of cutting fluids has shown to be effective and provides many advantages regarding, e.g., environmental protection and operator health [7]. The main challenge is to avoid overly high temperatures in the contact zone of the process to ensure long-term operability of the tool [8]. High temperatures are mainly caused by high mechanical friction between workpiece and worktool as well as poor thermal properties of the cutting fluid, in particular a low thermal conductivity [8]. Both properties can be improved when substituting liquids by nanofluids. In connection with grinding processes, for example, Shen et al. reported reduced grinding forces, an improved surface finish of the workpiece, and a reduction in friction as benefits [11]. In another study, Mao et al. [10] stressed the importance of large effective thermal conductivities and high lubrication powers of the cutting fluids. By this, the dry grinding performance was significantly improved with the use of MQL. Benefits from using water as cutting fluid were further enhanced when aluminium oxide (Al_2O_3) nanoparticles of 1.2 wt% mass fraction were added, which led to a larger thermal conductivity and better lubrication properties caused by the penetration of the particles into the grinding zone.

Until today, there is still a debate on the effective thermal conductivity λ_{eff} of nanofluids, both from an experimental and a theoretical perspective. While many studies [12–14] claim that a significant enhancement of the effective thermal conductivity can be achieved by the addition of nanoparticles to a fluid, other investigations [6, 15, 16] contradict this opinion. As shown in recent studies [6, 15, 17], the change in the thermal conductivity of a liquid by the addition of several volume or weight percent of particles is not anomalous, but only moderate and follows well the predictions from the classical Hamilton-Crosser (HC) model [18] or an analytical resistance model developed at AOT-TP [15, 19]. This could be demonstrated by the application of experimental techniques, such as the transient hot-wire method [6] or the steady-state parallel-plate method [15], in an adequate way, i.e. by realizing the theoretical description of the heat transfer via thermal

conduction as close as possible in the experiments. Thus, future investigations on λ_{eff} of nanofluids should aim to address the influencing factors such as, e.g., the thermal conductivities of the particles and the base fluid as well as the morphology and internal structure of the particles. While most research on nanofluids focuses on water and ethylene glycol as underlying base fluids, glycerol featuring a similar thermal conductivity as ethylene glycol, but a distinctly larger viscosity has been considered only in a few studies [20–22]. Regarding metal-oxide nanoparticles dispersed in liquids, copper, alumina, titania, and silica in its crystalline form are commonly studied [6, 15, 16].

The main objective of the present work is to provide reliable experimental data for the effective thermal conductivity consisting of quartz or amorphous SiO_2 or monoclinic ZrO_2 nanoparticles dispersed in a mixture of water and glycerol with a mass ratio of 60:40. Such nanofluids are considered as possible cutting fluids because they are based on a liquid continuous phase with a relatively large thermal conductivity and viscosity, in combination with nanoparticle types that are easily available. For the experimental determination of λ_{eff} of the three types of nanofluids, a steady-state technique in the form of a guarded parallel-plate instrument was used at temperatures between (293 and 353) K and a maximum particle volume fraction of 0.10. Furthermore, turbidity, scanning transmission electron microscopy (STEM), and dynamic light scattering (DLS) measurements allowed to qualitatively characterize the stability and dimensions of the dispersed non-spherical particles previously prepared in a top-down comminution step. The influence of temperature as well as volume fraction, thermal conductivity, and morphology of the particles on the measured thermal-conductivity ratios are discussed and used for comparison with predictions from the HC model [18] and an analytical resistance model [15, 19].

2 Experimental

2.1 Materials and Sample Preparation

As starting materials for the comminution step, three commercial metal-oxide powders, i.e. quartz SiO_2 (c-SiO_2), amorphous SiO_2 (a-SiO_2), and monoclinic ZrO_2 (m-ZrO_2), were used as provided by the manufacturers. Detailed information about the characteristics of the initial particles is given in Table 1. Here, the d_{50} value, i.e. the value of the particle diameter corresponding to 50 % in the cumulative particle size distribution, is in the µm range for c-SiO_2 and m-ZrO_2. The used a-SiO_2 particles have primary particle sizes of about 12 nm and were manufactured by continuous flame hydrolysis. In this step, loosely bound agglomerates as well as merged aggregates are formed, where sizes up to about 40 µm are characteristic for the powder starting material as stated by the manufacturer.

To obtain the nanofluids, comminution was carried out in a planetary ball mill (PM400, Retsch, Germany) using water as dispersion medium and a milling speed of 400 rpm over a period between (3 and 7) h. The grinding balls were made of ZrO_2 with a diameter between (280 and 400) µm and their amount was calculated in order

Table 1 Properties of the initial particles before the comminution process [23–26]

Particle type	Trade name	CAS number	Provider	Purity in wt%	Major impurity in wt%	d_{50}/nm
Quartz SiO_2 (c-SiO_2)	SIKRON SF 800	14808–60-7	Quarzwerke group	97.5	Al_2O_3, 2	2000
Amorphous SiO_2 (a-SiO_2)	AEROSIL® 200 V	112945–52-5	Evonik industries	> 99.8	–	Primary: 12 Aggregates: average 157.5
Monoclinic ZrO_2 (m-ZrO_2)	ZirPro CC05	1314–23-4	Saint-Gobin	≥ 98	SiO_2, 0.5	1500

to obtain a filling bead ratio of 30 vol%. The accurate amount of particles and fluid were weighted using a precision balance (LA12000S, Sartorious, precision 0.1 g) to achieve particle mass fractions between 0.095 and 0.31 in water. To suppress particle agglomeration during comminution, the surface charge of the particles was increased. For this purpose, the pH of the two SiO_2-based nanofluids was adjusted to values above 7 by adding potassium hydroxide as base (KOH pellets from Merck in aqueous solution of a concentration of 1 mol·dm^{-3}). The estimated maximum mass fraction of KOH in water was 0.05, which is too small to detect a difference between the thermal conductivity of water and that of the solution. This statement is confirmed by the work of Riedel [27] and La Bideau et al. [28]. In the case of ZrO_2, the pH of the forming dispersions was already at 11, and did not require a further adjustment. After the comminution process, a defined amount of glycerol ($C_3H_8O_3$, Chemiekontor, purity ≥ 99.5 %) was added to the respective sample in order to obtain a mass ratio of 60:40 between water and glycerol.

The particle mass fractions w in the final nanofluids were converted to particle volume fractions φ based on the density of the water-glycerol base fluid ρ_{bf} [29] and of the particles ρ_p. For the true density of the particles, literature data for the bulk material at 298.15 K were collected for c-SiO_2 (ρ_p = 2650 kg·m^{-3}), a-SiO_2 (ρ_p = 2196 kg·m^{-3}) and m-ZrO_2 (ρ_p = 5680 kg·m^{-3}) [30]. The used approach assumes an ideal mixing behavior neglecting influences from further impurities. Taking into consideration the sample preparation procedure and the uncertainties associated with the input parameters, the relative expanded (coverage factor k = 2) uncertainties of the particle volume fractions and the volume fractions of the base fluid in all nanofluids studied are estimated to be 5% in both cases. For all three particle types, a volume fraction of about 0.03 was prepared. An additional concentration dependency was probed for the c-SiO_2-based nanofluid by preparing three further φ values of 0.05, 0.075, and 0.10. The detailed values for w and φ are given in Table 2 in connection with the measurement results for the effective thermal conductivity.

2.2 Characterization of Nanofluids

After the comminution process, different experimental techniques were applied at the Technische Universität Braunschweig (TUBS) for the characterization of the morphology and stability of the nanoparticles. The main information is given in the following section, while additional details are provided in the Supporting Information.

2.2.1 Dynamic Light Scattering

The nanofluids obtained directly after the comminution process, i.e. the particles dispersed in H_2O, were investigated by dynamic light scattering (DLS) using a commercial instrument (Zetasizer Nano ZS, Malvern). With such instruments, only qualitative information about the particle size and its distribution can be deduced by the application of the Stokes–Einstein equation [31] that is additionally in principle only valid for an infinite dilution of the particles, whilst high particle concentrations are used in the present study. For details on the application of the DLS technique for the characterization of size, size distribution, and also, in some cases, shape of the particles in dispersed systems, the reader is referred to the literature [15, 31–34]. In the present work, the particle size distributions for the different types of nanofluids were obtained by combining the translational particle diffusion coefficient measured at 25 °C via DLS at a defined scattering angle of 175° with the Stokes–Einstein equation, in which the viscosity of pure H_2O of 0.89 mPa·s [35] was employed. The results can be found in section S1 of the Supporting Information.

For all nanofluids, a polydispersity can be observed, where the majority of the particles are in the submicron range after the comminution process. The c-SiO_2 and m-ZrO_2 particles have an average diameter (d_{50}) of around (200 and 187) nm and show a relatively narrow particle size distribution, with a ratio d_{90}/d_{10} between (2.6 and 3.3) for the four c-SiO_2 samples and 2.7 for the m-ZrO_2 sample. In contrast, the distribution of a-SiO_2 is much broader ($d_{90}/d_{10} \approx 6.1$) and gives an average diameter of $d_{50} \approx 124$ nm. The latter value is larger than the primary particle size given by the manufacturer (about 12 nm). However, it needs to be stated that the synthesis via flame hydrolysis results in particle aggregates and strong agglomerates with a typical hydrodynamic size which is bigger than the size of primary particles but still in the submicron range. Even by dispersion in aqueous media with high shear forces, those aggregates and agglomerates cannot be broken and therefore particle sizes in the range of the primary particles cannot be observed in dispersions. The presence of even larger particles, partially with sizes above 1 µm, is related to further aggregation and agglomeration effects which can lead to particle sizes of around 40 µm for the starting material according to the manufacturer. A deeper and quantitative analysis about the size distribution analyzed by DLS cannot be drawn here.

Table 2 Measurement results for the thermal conductivity of the water/glycerol mixture (mass ratio 60:40) and the effective thermal conductivity of the related nanofluids containing c-SiO_2, a-SiO_2, or m-ZrO_2 nanoparticles including the corresponding thermal-conductivity ratios

System	w	φ	T/K	ΔT/K	λ_{bf} or λ_{eff}/ ($mW \cdot m^{-1} \cdot K^{-1}$)	$\lambda_{eff} \cdot \lambda_{bf}^{-1}$
$H_2O + C_3H_8O_3$	0	0	293.14	2.5	462.7	–
			313.14		474.1	-
			333.14		491.8	–
			353.15		510.8	–
			293.14	3.0	457.8	–
			313.14		474.7	–
			333.14		496.0	–
			353.14		512.1	–
c-$SiO_2 + H_2O + C_3H_8O_3$	0.030	0.069	293.14	3.0	478.0	1.048
			313.14		491.2	1.034
			333.14		509.9	1.038
			353.14		524.9	1.040
	0.050	0.113	293.14	3.0	499.2	1.090
			313.14		512.7	1.085
			333.14		529.4	1.083
			353.14		541.1	1.074
	0.076	0.165	293.14	3.0	523.2	1.138
			313.14		538.4	1.140
			333.14		555.4	1.136
			353.14		564.9	1.129
	0.100	0.212	293.14	3.0	545.8	1.182
			313.14		561.7	1.188
			333.14		575.6	1.180
			353.14		587.0	1.174
a-$SiO_2 + H_2O + C_3H_8O_3$	0.030	0.059	293.14	3.0	472.6	1.033
			313.14		485.3	1.022
			333.14		502.9	1.014
			353.15		519.6	1.015
m-$ZrO_2 + H_2O + C_3H_8O_3$	0.031	0.141	293.14	3.0	481.2	1.050
			313.14		496.6	1.051
			333.14		514.5	1.052
			353.15		526.5	1.045

The thermal-conductivity ratio $\lambda_{eff} \cdot \lambda_{bf}^{-1}$ is calculated using the thermal conductivity λ_{bf} of the base fluid measured directly before each nanofluid sample. This value for λ_{bf} can be slightly different from the λ_{bf} data shown in the table which refer to an exemplary measurement series

2.2.2 Scanning Transmission Electron Microscopy

For the final nanofluids featuring the water/glycerol mixture as base fluid, scanning transmission electron microscopy (STEM) was applied using a Helios 5 UX

instrument (Thermo Fisher). Representative STEM images for the dried particles based on nanofluids with $\varphi = 0.03$ are given in Fig. 1 and confirm the qualitative DLS measurements results that the majority of the particles in all systems are smaller than 1 µm and a clear polydispersity can be observed. The c-SiO_2 and m-ZrO_2 particles represent statistically distributed, non-spherical fragments with dimensions on the order of about (50 to 200) nm that are mainly present as primary particles and resulted from the comminution of clearly larger particles; see Table 1. For the sample with the largest c-SiO_2 concentration ($\varphi = 0.10$), no clear differences of the STEM images to those related with $\varphi = 0.03$ can be found, indicating that there is no significant difference in the agglomeration state of the nanoparticles at higher concentration. In the case of a-SiO_2, the primary spherical particles are much smaller than for the other two particle types and cannot be evaluated properly by STEM. As expected, most of the particles are aggregated and have a tendency to build even bigger agglomerates of irregular shape. Whilst in the comminution process those agglomerates and aggregates are partially broken, it seems that a fast re-agglomeration takes place.

Since the particle morphology is a key influencing parameter for λ_{eff} and required in common modeling approaches, a further evaluation of the STEM images was made using ImageJ software (version 1.53 k) [36]. As indicator for the particle shape, the 2D circularity of the particles was calculated considering a broad ensemble of particles. Details of the calculation procedure are given in section S2 of the Supporting Information. A circularity value of 1 indicates a perfect circle, whereas values close to zero indicate an elongated non-spherical shape, i.e. a rod with a large length-to-width ratio. For c-SiO_2 and m-ZrO_2 nanoparticles, circularity values including standard deviations ($k = 1$) of 0.64 ± 0.17 and 0.63 ± 0.22 were obtained, respectively. In the case of a-SiO_2, the circularity could not be properly evaluated because no clear boundaries between the individual particles and corresponding aggregates/agglomerates could be defined; the resulting mean circularity of 0.38 ± 0.22 appears to be underestimated and form a lower boundary. Hence, we estimate that the particle circularity of a-SiO_2 is between 1 associated with the primary spherical particles and the derived average circularity of 0.38. These specified values for the 2D circularity were employed as estimates for the 3D sphericity Ψ, which is required as input in the two applied models for λ_{eff}.

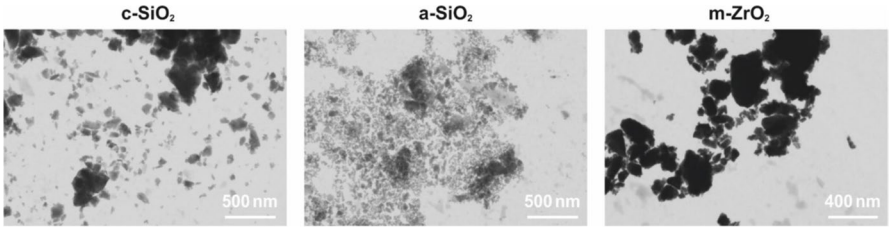

Fig. 1 STEM micrographs of the dried c-SiO_2 (left), a-SiO_2 (middle), and m-ZrO_2 (right) nanoparticles prepared from nanofluids with a particle volume fraction of 0.03 in the water/glycerol base fluid

2.2.3 Turbidity Measurements

For an accurate measurement of λ_{eff} of nanofluids, it is essential that the nanofluids remain stable and that the nanoparticles do not substantially sediment during the measurement. For this reason, the TurbiScan stability index (TSI) was recorded as a function of time for all water-glycerol-based nanofluids using a commercial instrument (TurbiScan Lab, Quantachrome GmbH & Co. KG) and can be seen in section S3 of the Supporting Information. Therein, also details on the measurements and the calculations of TSI can be found. TSI values below 1 indicate an excellent particle stability without visual destabilization [37, 38]. While TSI values between 1 and 3 imply a weak destabilization which might be visible in few cases, values larger than about 3 are associated with destabilization phenomena like sedimentation or creaming [38]. For the nanofluids containing a-SiO_2 ($\varphi = 0.03$) and c-SiO_2 ($\varphi = 0.03$–0.10), the TSI is below 3 for the period of the thermal-conductivity measurements of about 16 h. Such stability could also be observed by visual observation in glass flasks. In that case, the nanofluids started to show signs of destabilization although no significant change in the thermal conductivity was observed. The ZrO_2-containing nanofluid ($\varphi = 0.03$) shows the lowest stability, indicated by a TSI value of about 5.5 after 16 h. This means that the measurements for λ_{eff} of this sample may have been affected by destabilization effects. Although not clearly visible with the naked eye, one possible explanation for the lower stability and stronger sedimentation tendency may be the higher density of ZrO_2, which is more than double the density of SiO_2.

2.3 Effective Thermal Conductivity by Guarded Parallel-Plate Instrument

The effective thermal conductivity of the nanofluids λ_{eff} including the thermal conductivity of their related base fluid λ_{bf} was measured at ambient pressure with a newly developed guarded parallel-plate instrument (GPPI). This revised version is based on the same concept as the former measurement instrument detailed in Ref. [39]. In previous works, the GPPI has already been applied for the investigation of several types of fluids [39–42] including nanofluids [15]. A detailed description of the new apparatus will be given in a future study. In the present work, only the essential features of the instrument and the relevant experimental conditions and procedures are provided in the following.

The working principle of parallel-plate instruments for the measurement of the thermal conductivity is to fulfill the ideal one-dimensional form of the Fourier law of heat conduction for a planar sample, $\dot{Q}_{cond} = A \cdot \lambda \cdot \left(T_{hot} - T_{cold}\right)/s$, as close as possible. From an accurate determination of the heat flux $\dot{Q}_{cond}$ caused purely by conduction through the sample, the heat transfer area A, the sample thickness s, and the temperature difference $\Delta T = T_{hot} - T_{cold}$ between the two outer surfaces of the sample, the thermal conductivity of the sample λ can be directly accessed in an absolute and accurate way. For this, it needs to be ensured that additional contributions to the measured heat flux $\dot{Q}_{meas}$ due to advective heat transfer through the sample, heat leakages to the surrounding, or radiative heat transfer between the plates

in contact with the sample need to be suppressed as much as possible or taken into account in a reliable manner, which will be addressed below. Influences originating from the Soret and/or Dufour effect of the particles dispersed in nanofluids on $\dot{Q}_{\mathrm{meas}}$ are insignificant in connection with the used steady-state technique, as detailed in Ref. [15].

In the GPPI, advective heat transfer can be neglected for all measurements since the sample is placed between two parallel circular copper plates oriented perpendicular to the gravitational field and the heat flux is guided in a stable configuration from the upper hot to the lower cold plate. To suppress heat leakages from the balancing heating plate with diameter (86.00 ± 0.02) mm to the surrounding, the plate is covered by a multi-part guard system in lateral and radial direction. For this, each guard element of the heating system is controlled independently to the same temperature as the heating plate. Electrical resistance heating for the upper heating system and Peltier elements for the lower cooling plate are used for the control of the temperature field. The latter is recorded by several calibrated Pt100 resistance probes placed inside the GPPI and having an absolute uncertainty ($k=2$) of 0.02 K. A further guard around the multi-guard system is given by a housing made of aluminum alloy and featuring channels for the circulation of water. Its temperature was kept at about 1 K below T of the heating system by a lab thermostat. Radiative heat transfer between the surfaces of the heating and cooling are minimized by covering their polished surfaces with a thin chrome layer, i.e. the emission coefficient is reduced to about 0.04 [39]. Water [43] and glycerol [43] are relatively strongly absorbing fluids, i.e. radiation contributions are negligible, as shown in Ref. [39]. Since the investigated nanofluids are anticipated to absorb radiation even stronger than the base fluid, radiative heat transfer on the measurement results can be neglected. The measurement instrumentation and automation, sample preparation, and measurement procedure are basically identical as in our previous studies [15, 42] on λ_{bf} of water-based nanofluids using the old version of the GPPI. To adjust the layer thickness s, polyether ether ketone (PEEK) spacers with a thickness of (2 ± 0.02) mm were used in the present study.

The functionality of the new GPPI was validated by performing measurements on several liquids including water as reference fluid. For the latter liquid studied at mean T from (283 to 358) K, the measured results obtained for $s=$(1.5 and 2) mm in combination with temperature differences ΔT of (2.0, 2.5, and 3.0) K agree with the reference correlation from Huber et al. [44] recommended by the REFPROP database [45] with an average absolute deviation of 0.5 %, where the maximum and minimal deviations are − 0.8 % and 0.6 % at (283 and 358) K, respectively. The deviations are within the experimental uncertainty ($k=2$) of the present measurement data which can be specified with 3 % considering the uncertainties of the input parameters on the working equation. Details on these investigations will be provided in a future study.

Before the investigation of the nanofluids, the thermal conductivity λ_{bf} of the base fluid water/glycerol (60:40 wt%) was measured at mean T of (293, 313, 333, and 353) K using two values for $\Delta T=$(2.5 and 3.0) K between the two plate surfaces. For the study of the nanofluids, the larger $\Delta T=3.0$ K was selected at the same four mean T as the base fluid. Before each nanofluid measurement, λ_{bf} of the base fluid

was measured and used as a reference for the calculation of the thermal-conductivity ratio. For these six sets of measurement, agreement between the individual λ_{bf} values clearly within the expanded experimental uncertainty was achieved. For each nanofluid, the measurements were performed from the lowest to the highest T within a time period between (16 and 18) h. After the steady-state is reached, a total of 25 data points are collected for one temperature during a period of 10 min. Based on twice the standard deviation of the 25 data points, the repeatability of the thermal conductivity measurements is estimated to be 0.5 %. After opening the instrument, a visual inspection of the samples indicated no clear sedimentation or agglomeration for all studied nanofluids.

3 Results and Discussion

The following section summarizes and discusses the measurement results for the thermal conductivity of the base fluid and the effective thermal conductivity of the nanofluids, including corresponding thermal-conductivity ratios, as a function of temperature and composition. A comparison is made with a single data source in literature available for the base fluid and with two theoretical approaches for the prediction of λ_{eff}. In this context, the influence of the non-spherical morphology of the dispersed SiO_2 and ZrO_2 nanoparticles on the effective thermal conductivity is pointed out.

3.1 Summary of Measurement Results

The experimental results for λ_{bf} and λ_{eff} measured from (293 to 353) K with expanded uncertainties of 3 % are listed in Table 2. In the case of λ_{bf}, the thermal conductivities obtained by applying $\Delta T = (2.5$ and $3.0)$ K are given for each T based on one exemplary measurement set. Since λ_{eff} was only investigated using $\Delta T = 3.0$ K, due to consistency reasons the λ_{bf} values associated with the same ΔT served as a reference to calculate the thermal-conductivity ratio $\lambda_{eff} \cdot \lambda_{bf}^{-1}$, i.e. the ratio of the effective conductivity of the nanofluid to the thermal conductivity of the base fluid measured directly before the corresponding nanofluid. According to Gaussian error propagation, the $\lambda_{eff} \cdot \lambda_{bf}^{-1}$ ratio also listed in Table 2 for each thermodynamic state is associated with an expanded uncertainty of 4.2% ($k = 2$).

3.2 Thermal Conductivity of Base Fluid

The measured thermal conductivities λ_{bf} of the base fluid, i.e. a mixture of water and glycerol with a mass ratio of 60:40, are shown in Fig. 2 as a function of temperature, differentiating between the individual data sets related to $\Delta T = (2.5$ and $3.0)$ K. Both sets show agreement clearly within the experimental uncertainty ($k = 2$) of about 3 %, which confirms the reliability of the measurement instrument. The only further source in literature for λ_{bf} of the specific water/glycerol mixture is the correlation

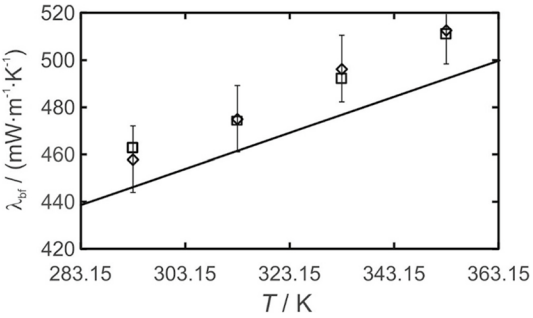

Fig. 2 Thermal conductivity of a mixture of water and glycerol (mass ratio 60:40) at atmospheric pressure measured by GPPI as a function of temperature: □, $\Delta T = 2.5$ K, measurement results from present study; ◇, $\Delta T = 3.0$ K, measurement results from present study; ——, correlation developed by Bates [46] from measurements with a parallel-plate method. For the experimental data, the error bars are only shown for $\Delta T = 3.0$ K

reported by Bates [46]. This linear *T*-dependent correlation was developed based on measurements with a parallel-plate method between (283 and 353) K, without a specification of the experimental uncertainty. As can be seen from Fig. 2, our present data are larger than the correlation of Bates [46] with a maximum relative deviation of 4.1 % and an average absolute relative deviation (AARD) of 3.4 %. However, both data sets show a very similar *T*-dependent trend. It should be mentioned that Bates' measurement results for pure water, forming the major component in the present base fluid, show negative deviations of up to − 1.3 % from the reference correlation [44] at a low *T* of 303.15 K, while the deviations are inverted to positive values at larger *T* with a value of + 2.5 % at 353.15 K. This trend may indicate a weak heat leakage from the guard system to the balancing heating plate at low *T*, corresponding to smaller heat fluxes, and vice versa at larger *T*, associated with somewhat larger heat fluxes. Since the heat fluxes measured for the water/glycerol base fluid are lower than for pure water in the case of a constant *T*-gradient used by Bates [46], it may explain his systematically lower values for λ_{bf} compared to the present work. Nevertheless, the agreement between both data sets is still reasonably good. Further experimental data for λ_{bf} are not available in the literature to the best of our knowledge.

3.3 Effective Thermal Conductivity of Nanofluids

In this section, the measurement results for the effective thermal conductivity of the three different nanofluids are discussed in terms of the thermal-conductivity ratio $\lambda_{eff} \cdot \lambda_{bf}^{-1}$. Since further experimental results for λ_{eff} of the present nanofluids are not available in the literature to the best of our knowledge, for comparison we applied two common prediction models, i.e. the Hamilton-Crosser (HC) model [18] and an analytical resistance model [15], called AOT-TP model in the following. Details to these two models can be found in the cited references. As input for both models, the thermal conductivities of the base fluid λ_{bf} and the morphology of the particles,

i.e. their mean diameter d_{50} extracted from the DLS measurements and their sphericities Ψ estimated directly from the STEM-based circularities, are employed from the experimental results. Furthermore, the thermal conductivities of the c-SiO_2 (λ_p = (1.30 to 1.58) $W \cdot m^{-1} \cdot K^{-1}$ from (273 to 450) K) [47], a-SiO_2 (λ_p = (1.40 to 1.80) $W \cdot m^{-1} \cdot K^{-1}$ from (273 to 463) K) [30], and m-ZrO_2 (λ_p = 2.0 $W \cdot m^{-1} \cdot K^{-1}$ from (373 to 673) K [30]; value also employed for lower T studied in this work) particles are taken from the literature and correlated with a linear T-dependent fit. Additional parameters required in the AOT-TP model and adopted from the literature are the densities of the particles, as stated in Sect. 2.1, and the thermal diffusivity of the base fluid. Although no information about the latter property is available, it has been estimated by using data for the density of the mixture [29], the heat capacity of the two pure fluids [45, 48] averaged according to their mass fractions in the base fluid, and the measured thermal conductivity λ_{bf} reported in Table 2. Even if the thermal diffusivity is under- or overestimated by 50%, the absolute variation of λ_{eff} is smaller than 0.1 % in the exemplary case of the c-SiO_2-based nanofluid with $\varphi = 0.10$ at $T = 298.15$ K.

Figure 3 shows the temperature dependency for the experimental (markers) and modeled (lines) results for $\lambda_{eff} \cdot \lambda_{bf}^{-1}$ of the three nanofluids at a constant particle volume fraction $\varphi = 0.03$. In connection with the HC model and AOT-TP model visualized in columns (a) and (b) of the figure, respectively, the solid lines correspond to the values for the average sphericities Ψ, while the dotted and dashed lines reflect the models corresponding to the upper and lower boundaries of Ψ, i.e. the uncertainties as obtained by STEM. In the case of a-SiO_2, where the evaluation of the STEM images was hardly possible, only the two boundaries corresponding to $\Psi = 1$ and $\Psi = 0.38$ are given in Fig. 3. Here, it can be seen that moderate thermal-conductivity ratios between about 1.02 and 1.05 could be resolved by the measurements for all three nanofluids, independent of temperature and particle type. The latter behavior can be related to the fact that all three particles have similar particle thermal conductivities λ_p and, in turn, similar $\lambda_p \cdot \lambda_{bf}^{-1}$ ratios of about 2.9 (a-SiO_2), 3.1 (c-SiO_2), and 4.4 (m-ZrO_2).

In all cases, agreement between the experimental results and the two prediction models within the experimental uncertainties and the confidence level of the models is found. By trend, the experimental results for c-SiO_2 and m-ZrO_2 agree better with the HC model that provides larger $\lambda_{eff} \cdot \lambda_{bf}^{-1}$ values than the AOT-TP model. The latter is apparently superior to the HC model in the case of the nanofluid featuring a-SiO_2 particles. Our previous study on water-based nanofluids containing nearly spherical titanium oxide (TiO_2), SiO_2, or polystyrene (PS) particles indicated that the AOT-TP model is often superior to the HC model to describe $\lambda_{eff} \cdot \lambda_{bf}^{-1}$ for these systems. Similar conclusions can also be deduced by considering the review [17] and experimental study [6] from the research groups of Wakeham and Assael. Thus, the results from the present work and the literature suggest that the HC model seems to be more reliable for nanofluids with base fluids of relatively large viscosity such as the present water/glycerol mixture ($\eta = 3.63$ mPa·s at 293.15 K [29]) or ethylene glycol ($\eta = 20.9$ mPa·s at 293.15 K [45]), while the AOT-TP model can be superior in the case of low-viscosity base fluids such as water ($\eta = 1.00$ mPa·s at 293.15 K

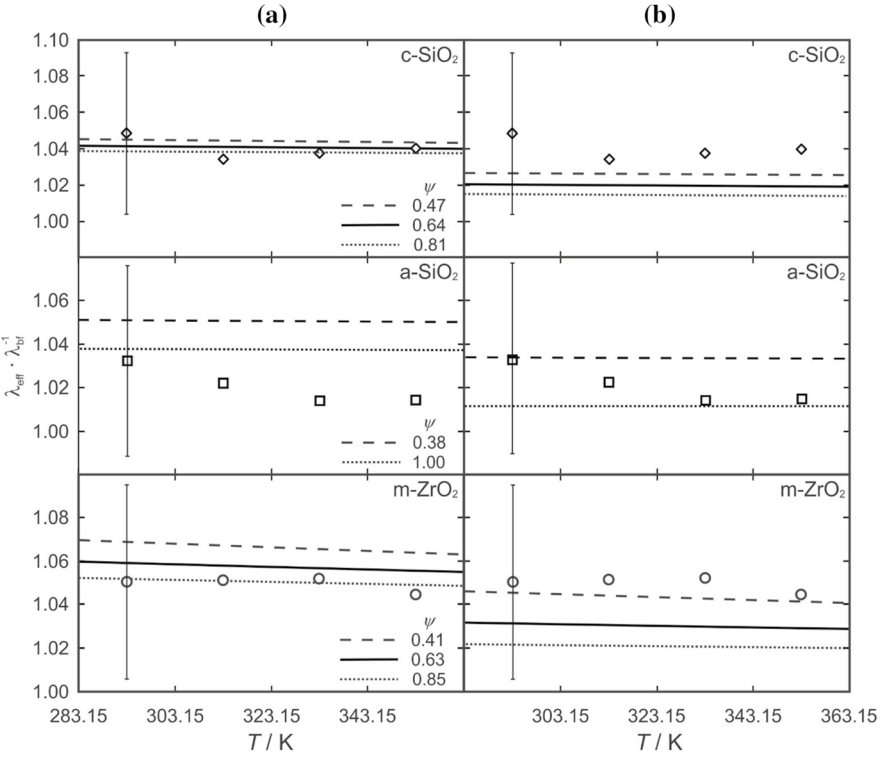

Fig. 3 Thermal-conductivity ratio for nanofluids containing c-SiO_2 (top row), a-SiO_2 (middle row), and m-ZrO_2 (bottom row) particles dispersed in a mixture of water and glycerol (mass fraction 60:40) as a function of temperature at $\varphi = 0.03$ comparing the experimental results with predictions from the HC model (column a) and the AOT-TP model (column b): ◇, □, and ○, measurement; ——, models using average particle sphericity derived from STEM; ····· and – – –, models representing the higher and lower boundaries of particle sphericity. Error bars represent the experimental ($k = 2$) uncertainty of the thermal-conductivity ratio, which are shown exemplarily for one temperature in each case

[35]). Both models predict also no T-dependency for $\lambda_{eff} \cdot \lambda_{bf}^{-1}$ in the probed T range, which is confirmed by our experimental results.

For the nanofluid containing the c-SiO_2 particles, the concentration dependency of the effective thermal conductivity was additionally studied at T between (293.15 and 353.15) K in steps of 20 K. For an exemplary temperature of 293.15 K, the measurement results for $\lambda_{eff} \cdot \lambda_{bf}^{-1}$ are illustrated in the upper part of Fig. 4 together with the predictions by the HC model and AOT-TP model in columns (a) and (b). Based on the measurements, a relatively linear increase of the thermal-conductivity ratio up to about 1.18 at $\varphi = 0.10$ is found. This behavior is similar for all studied temperatures, as can be seen in Fig. S4 of the Supporting Information. These results and those shown in Fig. 3 demonstrate again that a rise in temperature associated with an intensification of the Brownian motion of the particles does not cause a significant change in the $\lambda_{eff} \cdot \lambda_{bf}^{-1}$ ratio.

In accordance with the observations made in Fig. 3, the HC model is in better agreement with the experimental data within their expanded uncertainties than the AOT-TP model that underestimates the effective thermal conductivity, especially at the largest φ. Furthermore, both models predict no temperature dependence for $\lambda_{eff} \cdot \lambda_{bf}^{-1}$ within the studied T range, which can be observed from Fig. S4 of the Supporting Information. For a proper application of the two models, detailed information about the average sphericity of the non-spherical c-SiO_2 particles ($\Psi = 0.64 \pm 0.17$), as revealed by the STEM images in Fig. 1, is required. If a sphericity $\Psi = 1$ related to spherical particles is used, the predictions for $\lambda_{eff} \cdot \lambda_{bf}^{-1}$ would be systematically too low in both cases. An increase in the thermal-conductivity ratio with decreasing Ψ, i.e. increasing deviations from a sphericity of the particles of same volume, can be rationalized by the increasing surface area of the particles. This larger heat transfer area results in a larger convective heat transfer between particles and fluid, as it is reflected by the AOT-TP model [15, 19].

In the calculation of the modeled values displayed in the upper part of Fig. 4, it has been assumed that the present nanofluid features solely c-SiO_2 particles

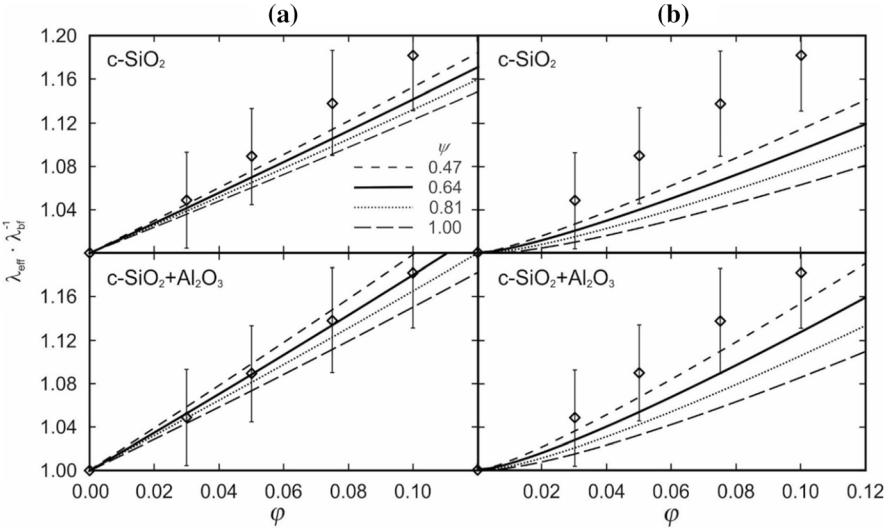

Fig. 4 Thermal-conductivity ratio for nanofluid containing a-SiO_2 particles dispersed in a mixture of water and glycerol (mass ratio 60:40) as a function of the particle volume fraction at $T = 293.15$ K comparing the experimental results with predictions from the HC model (column a) and the AOT-TP model (column b): ◇, measurement; ——, models using average particle sphericity derived from STEM; ····· and – – –, models representing the upper and lower boundaries of particle sphericity; — —, models in case of spherical particles with a particle sphericity of 1. In the top row, λ_p used in the two models corresponds to that for pure c-SiO_2 ($\lambda_p = 1.35$ W·m^{-1}·K^{-1}). In the bottom row, $\lambda_p = 1.7$ W·m^{-1}·K^{-1} used in the two models corresponds to the volume-weighted average of the λ_p values for a binary mixture of c-SiO_2 ($\lambda_p = 1.35$ W·m^{-1}·K^{-1}, volume fraction 0.985) and Al_2O_3 ($\lambda_p = 23.5$ W·m^{-1}·K^{-1}, volume fraction 0.015), representing the influence of the Al_2O_3 impurities in the sample. Error bars represent the experimental ($k = 2$) uncertainty of the thermal-conductivity ratio

featuring a thermal conductivity of $\lambda_p \approx 1.35$ W·m^{-1}·K^{-1}. However, according to the specification of the manufacturer, the original powder shows only a mass fraction purity of 0.975 and includes alumina (Al_2O_3) as a major impurity with $w = 0.02$ and a distinctly larger λ_p value of 23.5 W·m^{-1}·K^{-1}, which represents the mean average of (30 and 17) W·m^{-1}·K^{-1} for particle densities of 3800 or 3500 kg·m^{-3}, respectively, at 373.15 K [30]. Thus, as input for the models, we have calculated a volume-weighted average for the thermal conductivity of the particle mixture ($\lambda_p \approx 1.7$ W·m^{-1}·K^{-1}), assuming mass fractions of 0.98 for c-SiO_2 and 0.02 for Al_2O_3 and considering the particle density for c-SiO_2 ($\rho_p = 2650$ kg·m^{-3}) and Al_2O_3 ($\rho_p = 3650$ kg·m^{-3} as average value). As can be seen from the lower part of Fig. 4 for $T = 293.15$ K, the predictions from both models considering the presence of Al_2O_3 in the particle ensemble increase relative to those neglecting this, which makes up to 3.4 % and 3.0 % changes for $\lambda_{eff} \cdot \lambda_{bf}^{-1}$ in case of the HC and AOT-TP models, respectively, for $\Psi = 0.64$ and $\varphi = 0.10$. Over the entire composition range, the experimental data are represented well by both updated models, in particular the HC model, which is also the case for all other T according to Fig. S5 in the Supporting Information and corroborates the previous findings shown in Fig. 3. Here, at the lowest concentration of $\varphi = 0.03$, the changes between the modeling results considering and omitting the presence of Al_2O_3 are within 1 % and do not have a pronounced effect yet. Nevertheless, the current example demonstrates that besides a reasonable information about the morphology of the particles, also data on their thermal conductivity is essential for reliable predictions of the effective thermal conductivity of nanofluids.

4 Conclusions

The present work has investigated the effective thermal conductivity λ_{eff} of nanofluids comprised of silica and zirconium dioxide nanoparticles dispersed in a high-viscosity mixture of water and glycerol with a mass ratio of 60:40. For these nanofluids, being of potential interest in tribological applications, measurements were performed at ambient pressure from (293 to 353) K with a new version of a steady-state guarded-parallel plate instrument that is designed to represent the one-dimensional Fourier law of heat conduction as close as possible. The experimental thermal conductivities λ_{bf} of the base fluid agree well with a single data source in the literature. At a constant volume fraction of the c-SiO_2, a-SiO_2, and m-ZrO_2 nanoparticles with a value of 0.03, the measured thermal-conductivity ratios $\lambda_{eff} \cdot \lambda_{bf}^{-1}$ show moderate values around 1.05 and are independent of the particle type and temperature. A concentration-dependent study on the nanofluids containing the crystalline SiO_2 particles revealed a linear and T-invariant increase of $\lambda_{eff} \cdot \lambda_{bf}^{-1}$. The application of two common prediction models for λ_{eff} of the present nanofluids with relatively large viscosities indicated overall a better performance of the HC model compared to an analytical resistance model developed at AOT-TP. A better accuracy of the models is achieved when considering the information about the circularity or sphericity of the dispersed particles of rather

irregular non-spherical shape as well as the presence of particle impurities which can affect the average thermal conductivity of the dispersed phase. Further systematic studies need to be conducted in the future in order to analyze the trend that the HC model and AOT-TP model appear to be more suitable for the prediction of λ_{eff} of nanofluids having relatively large and small viscosities of the base fluid, respectively.

Supplementary Information The online version contains supplementary material available at https://doi.org/10.1007/s10765-022-03084-z.

Acknowledgements The authors gratefully acknowledge funding of the Erlangen Graduate School in Advanced Optical Technologies (SAOT) by the Bavarian State Ministry for Science and Art. The authors gratefully thank Sherif Okeil for supporting the STEM analysis.

Author Contributions FEBB measured the thermal conductivity and wrote the main manuscript text, CK prepared and characterized the nanofluids, and TMK and APF wrote the main manuscript text. All authors reviewed the manuscript.

Funding Open Access funding enabled and organized by Projekt DEAL. This work was funded by the Deutsche Forschungsgemeinschaft (DFG, German Research Foundation) via the project grants FR 1709/20-1 and GA 1492/16-1 (Project Number 426927572).

Data Availability Not applicable.

Declarations

Conflict of interest The authors have no competing interests as defined by Springer, or other interests that might be perceived to influence the results and/or discussion reported in this paper.

References

1. S. U. S. Choi, J. A. Eastman, in *Proceedings of the ASME International Mechanical Engineering Congress and Exposition*, vol. **66** (1995), p. 99.
2. R. Faridi Khouzestani, A. Ghafouri, SN Appl. Sci. **2**, 298 (2020)
3. V. Mikkola, S. Mikkola, H. Granbohm, K. Saari, T. Ala-Nissila, A. Seppälä, in *12th International Conference on Heat Transfer, Fluid Mechanics and Thermodynamics* (Spain, 2016).
4. A. Bhattad, J. Sarkar, P. Ghosh, Renew. Sustain. Energy Rev. **82**, 3656 (2018)
5. M.H. Buschmann, R. Azizian, T. Kempe, J.E. Juliá, R. Martínez-Cuenca, B. Sundén, Z. Wu, A. Seppälä, T. Ala-Nissila, Int. J. Therm. Sci. **129**, 504 (2018)
6. G.J. Tertsinidou, C.M. Tsolakidou, M. Pantzali, M.J. Assael, L. Colla, L. Fedele, S. Bobbo, W.A. Wakeham, J. Chem. Eng. Data **62**, 491 (2017)
7. Z. Said, M. Gupta, H. Hegab, N. Arora, A.M. Khan, M. Jamil, E. Bellos, Int. J. Adv. Manuf. Technol. **105**, 2057 (2019)

8. A.K. Sharma, A.K. Tiwari, A.R. Dixit, Mater. Today Proc. **2**, 3545 (2015)
9. B. Shen, A.J. Shih, S.C. Tung, Tribol. Trans. **51**, 730 (2008)
10. C. Mao, X. Tang, H. Zou, X. Huang, Z. Zhou, Int. J. Precis. Eng. Manuf. **13**, 1745 (2012)
11. B. Shen, P. Kalita, A.P. Malshe, A.J. Shih, Trans North Am. Manuf. Res. Inst. SME **36**, 8 (2008)
12. P.B. Maheshwary, C.C. Handa, K.R. Nemade, Appl. Therm. Eng. **119**, 79 (2017)
13. D. Mitra, P. Howli, B.K. Das, N.S. Das, P. Chattopadhyay, K.K. Chattopadhyay, J. Mol. Liq. **302**, 112499 (2020)
14. S.M.S. Murshed, K.C. Leong, C. Yang, Int. J. Therm. Sci. **44**, 367 (2005)
15. F.E. Berger Bioucas, M.H. Rausch, J. Schmidt, A. Bück, T.M. Koller, A.P. Fröba, Int. J. Thermophys. **41**, 55 (2020)
16. M.H. Buschmann, Int. J. Therm. Sci. **62**, 19 (2012)
17. G. Tertsinidou, M.J. Assael, W.A. Wakeham, Int. J. Thermophys. **36**, 1367 (2015)
18. R.L. Hamilton, O.K. Crosser, Ind. Eng. Chem. Fundam. **1**, 187 (1962)
19. K.N. Shukla, T.M. Koller, M.H. Rausch, A.P. Fröba, Int. J. Heat Mass Transf. **99**, 532 (2016)
20. M.C. Lahari, P.S. Sai, K.V. Sharma, K.S. Narayanaswamy, Mater. Today Proc. (2022). https://doi.org/10.1016/j.matpr.2022.05.284
21. S. Harikrishnan, A.A. Roseline, S. Kalaiselvam, IEEE Trans. Nanotechnol. **12**, 629 (2013)
22. N. Tshimanga, M. Sharifpur, J.P. Meyer, Heat Transf. Eng. **37**, 1538 (2016)
23. *Product Data SIKRON® Quartz* (Quarzwerke GmbH, n.d.), p. 2.
24. *Produt Information AEROSIL® 200* (Evonik Resource Efficiency GmbH, 2019), p. 2.
25. *CC Zirconia Technical Data Sheet* (Saint-Gobain Zirpro, 2020), p. 1.
26. Evonik Industries AG, *AEROSIL® – Fumed Silica Technical Overview* (2015).
27. L. Riedel, Chem. Ing. Tech. **23**, 59 (1951)
28. D. Le Bideau, P. Mandin, M. Benbouzid, M. Kim, M. Sellier, Int. J. Hydrog. Energy **44**, 4553 (2019)
29. K. Takamura, H. Fischer, N.R. Morrow, J. Pet. Sci. Eng. **98–99**, 50 (2012)
30. D.R. Lide, *CRC Handbook of Chemistry and Physics, Internet Version 2005* (CRC Press, Boca Raton, FL, 2005)
31. B.J. Berne, R. Pecora, *Dynamic Light Scattering: With Applications to Chemistry, Biology, and Physics* (Dover Publications, Mineola, 2000)
32. F.E. Berger Bioucas, C. Damm, W. Peukert, M.H. Rausch, T.M. Koller, C. Giraudet, A.P. Fröba, J. Phys. Chem. B **123**, 9491 (2019)
33. S. Bi, T.M. Koller, M.H. Rausch, P. Wasserscheid, A.P. Fröba, Ind. Eng. Chem. Res. **54**, 3071 (2015)
34. M.S.G. Knoll, C. Giraudet, C.J. Hahn, M.H. Rausch, A.P. Fröba, J. Colloid Interface Sci. **544**, 144 (2019)
35. M.L. Huber, R.A. Perkins, A. Laesecke, D.G. Friend, J.V. Sengers, M.J. Assael, I.N. Metaxa, E. Vogel, R. Mareš, K. Miyagawa, J. Phys. Chem. Ref. Data **38**, 101 (2009)
36. C.A. Schneider, W.S. Rasband, K.W. Eliceiri, Nat. Methods **9**, 671 (2012)
37. Formulaction Smart Scientific Analysis, Turbiscan Stability Index (TSI)—Stability Evaluation with Just One Click (n.d.), p. 2.
38. *Turbiscan Stability Scale - The Stability Criteria and Correlation to Visual Observation*.https://formulaction.com/wp-content/uploads/2022/08/AN-Quantify-Stability-with-TSI-Scale-.pdf. Accessed July 15, 2022
39. M.H. Rausch, K. Krzeminski, A. Leipertz, A.P. Fröba, Int. J. Heat Mass Transf. **58**, 610 (2013)
40. A.P. Fröba, M.H. Rausch, K. Krzeminski, D. Assenbaum, P. Wasserscheid, A. Leipertz, Int. J. Thermophys. **31**, 2059 (2010)
41. T.M. Koller, S.R. Schmid, S.J. Sachnov, M.H. Rausch, P. Wasserscheid, A.P. Fröba, Int. J. Thermophys. **35**, 195 (2014)
42. F.E. Berger Bioucas, M. Piszko, M. Kerscher, P. Preuster, M.H. Rausch, T.M. Koller, P. Wasserscheid, A.P. Fröba, J. Chem. Eng. Data **65**, 5003 (2020)
43. Coblentz Society, Inc., NIST Chem. WebBook NIST Stand. Ref. Database Number 69 (2022).
44. M.L. Huber, R.A. Perkins, D.G. Friend, J.V. Sengers, M.J. Assael, I.N. Metaxa, K. Miyagawa, R. Hellmann, E. Vogel, J. Phys. Chem. Ref. Data **41**, 033102 (2012)
45. E.W. Lemmon, I.H. Bell, M.L. Huber, M.O. Linden, *REFPROP*, Standard Reference Data Program, version 10.0; National Institute of Standards and Technology (NIST): Gaithersburg, MD, USA (2018)
46. O.K. Bates, Ind. Eng. Chem. **28**, 494 (1936)

47. O.A. Sergeev, A.G. Shashkov, A.S. Umanskii, J. Eng. Phys. **43**, 1375 (1982)
48. M. Bastos, S.-O. Nilsson, M.D.M.C. Ribeiro da Silva, M.A.V. Ribeiro da Silva, I. Wadsö, J. Chem. Thermodyn. **20**, 1353 (1988)

Authors and Affiliations

Francisco E. Berger Bioucas[1] · Christian Köhn[2] · Annelise Jean-Fulcrand[2] · Georg Garnweitner[2] · Thomas M. Koller[1] · Andreas P. Fröba[1]

[1] Institute of Advanced Optical Technologies − Thermophysical Properties (AOT-TP), Department of Chemical and Biological Engineering (CBI) and Erlangen Graduate School in Advanced Optical Technologies (SAOT), Friedrich-Alexander-Universität Erlangen-Nürnberg (FAU), Paul-Gordan-Straße 8, 91052 Erlangen, Germany

[2] Institute for Particle Technology, Technische Universität Braunschweig (TUBS), Volkmaroder Straße 5, 38104 Brunswick, Germany